

# Impacts of the decreased freeze-up period on primary production in Qinghai Lake

Lian Feng<sup>a,b</sup>, Junguo Liu<sup>a</sup>, Tarig A. Ali<sup>c</sup>, Junsheng Li<sup>d</sup>, Juan Li<sup>e</sup>, Xingxing Kuang<sup>a,\*</sup>

<sup>a</sup> Guangdong Provincial Key Laboratory of Soil and Groundwater Pollution Control, School of Environmental Science and Engineering, Southern University of Science and Technology, Shenzhen, China

<sup>b</sup> Shenzhen Municipal Engineering Lab of Environmental IoT Technologies, Southern University of Science and Technology, Shenzhen 518055, Guangdong Province, China

<sup>c</sup> Geospatial Analysis Center, College of Engineering, American University of Sharjah, 26666, United Arab Emirates

<sup>d</sup> Key Laboratory of Digital Earth Science, Institute of Remote Sensing and Digital Earth, Chinese Academy of Sciences, Beijing, China

<sup>e</sup> Chinese Antarctic Center of Surveying and Mapping, Wuhan University, Wuhan 430079, China

## ARTICLE INFO

### Keywords:

Chl-a  
nFLH  
ABI  
Ocean color  
Ice cover  
Remote sensing  
MODIS  
VIIRS

## ABSTRACT

Although previous research has focused on the inundation changes in Qinghai Lake, the largest lake in China, few studies have investigated the variations in primary production and correlated these changes with environmental transitions. In this study, this knowledge gap was filled using multiple ocean color satellite missions between 2003 and 2017. The results indicated a substantial increase in phytoplankton growth over recent years, during which the normalized fluorescence line height (nFLH) and algal bloom index (ABI) increased by approximately 45% and 61%, respectively, from the first (2003–2012) to the second period (2013–2017). Such a remarkable increase is likely associated with a rapid decrease in the duration of the freeze-up period, for which the 2014–2017 mean was > 2 standard deviations below that of the previous years. High temperatures and a large number of sunshine hours could possibly explain the elevated nFLH and ABI in 2013. A multiple general linear model revealed that the freeze-up period, number of sunshine hours, and temperature explained 76.1%, 5.6%, and 10.2%, respectively, of the long-term changes in primary production in Qinghai Lake during the observed period. This study not only provides the first comprehensive analysis of the biogeochemical properties of Qinghai Lake but also demonstrates the capability of multiple remote sensing products in addressing environmental problems. Further, the method here is easily extendable to similar water bodies worldwide to study their potential responses to climate variability.

## 1. Introduction

Driven by both climate and anthropogenic forces, global surface waters have experienced considerable changes in recent decades (Pekel et al., 2016; Kraemer et al., 2017). For example, various lakes have disappeared in the Arctic driven by the thaw of the warming permafrost (Smith et al., 2005). In addition, the surface water resources in Iran, Afghanistan and Iraq have experienced significant decreases in recent years, primarily due to unregulated water withdrawal and hydrological alterations by dams and other hydraulic projects (Pekel et al., 2016). Similarly, the lakes atop the Tibetan Plateau, where significant area expansions have been demonstrated through various techniques, have not been immune to these changes (Song et al., 2014).

Qinghai Lake with a surface area of approximately 4000 km<sup>2</sup> and a mean depth of 21 m is the largest lake on the Tibetan Plateau and in China. With an elevation of approximately 3196 m above sea level, the

environmental changes in Qinghai Lake are considered important indicators of natural climate variability because of the limited impacts of human activities therein (Song et al., 2014; Liu and Chen, 2000; Shi and Ren, 1990).

Considerable research has focused on the dynamics of Qinghai Lake in terms of its size, ice cover, etc. For example, evidence indicates that Qinghai Lake exhibited a rapid reduction in size before the 2000s, followed by a significant expansion over the last decade (Dong and Song, 2011; Zhang et al., 2011; Li et al., 2007). These changes were primarily associated with global warming and wet/dry hydrological transitions locally. Furthermore, ice cover recession in the lake that manifested as delayed freeze-up and advanced ablation was revealed through both optical and microwave remote sensing techniques (Cai et al., 2017; Zhang et al., 2014; Wenbin et al., 2014). Indeed, the success of previous studies in this lake has relied primarily on the advantages of remote sensing techniques (such as synoptic, continuous

\* Corresponding author.

E-mail address: [kuangxx@sustech.edu.cn](mailto:kuangxx@sustech.edu.cn) (X. Kuang).

observations) partly because the lake's high altitude presents a challenge to the acquisition of field data.

Satellite imagery has been widely used to monitor and understand the physical and hydrological characteristics of Qinghai Lake as well as many other alpine lakes throughout the Tibetan Plateau. However, few efforts have been made to examine the biogeochemical properties of Qinghai Lake that are considered to be more directly related to lake ecology (Dong et al., 2006). The existing studies performed in Qinghai Lake on biogeochemical parameters (e.g., chlorophyll (Chl)-a, dissolved oxygen, phosphorus, and nitrogen) were based mostly on field samples from a few cruise surveys (Bi et al., 2018). Nevertheless, the limited spatial and temporal representations of these datasets inhibited a full assessment of their spatiotemporal variability; consequently, the relationships between these variations and the aforementioned environmental transitions observed by satellites were not investigated.

The availability of decades of ocean color products from multiple missions (the Sea-viewing Wide Field-of-view Sensor (SeaWiFS), Moderate Resolution Imaging Spectroradiometer (MODIS), Visible Infrared Imaging Radiometer Suite (VIIRS), Medium Resolution Imaging Spectrometer (MERIS), Sentinel-3 Ocean and Land Colour Instrument (OLCI), etc.) has made it possible to quantify and understand the biogeochemical changes in waters at both global and regional scales (McClain, 2009; Wang et al., 2012). Therefore, ocean color measurements are expected to be useful for monitoring water constituents in large lakes, such as Qinghai Lake. Particularly useful are the standard ocean color algorithms that were developed using datasets collected from coastal or open oceans (O'Reilly et al., 1998; Werdell and Bailey, 2005), where the optical properties of salty alpine lakes are likely to be included. Unfortunately, these products have never been used on these remote lakes. Therefore, the current study was designed to (1) comprehensively monitor water primary production changes in Qinghai Lake using observations from multiple ocean color missions, (2) interpret such changes based on various environmental factors, and (3) demonstrate the benefits of using ocean color products in a high-altitude lake and the potential to extend these products to similar lakes.

## 2. Study area and environmental setting

Qinghai Lake is located in northeastern Qinghai (36°32'–37°15'N, 99°36'–100°47'E), a province in western China (see location in Fig. 1) (Immerzeel et al., 2010). Qinghai Lake is the largest lake in China, and its surface area has increased considerably in recent years (Song et al., 2014; Zhang et al., 2011). It is classified as a saline lake and a typical endorheic system; water from twenty-three rivers and streams (the largest tributary, Buha River, is annotated in Fig. 1) converges into Qinghai Lake, and the equilibration of the water budget mainly occurs through local evaporation (Rhode et al., 2010). The annual mean precipitation of the local area is ~360 mm, and the annual mean temperature is -0.7 °C (Colman et al., 2007; Yan et al., 2002). Due to the low temperature, the lake often remains completely frozen during several months of the year, although the ice cover duration has diminished over recent decades (Cai et al., 2017).

## 3. Datasets and methods

Five types of datasets, namely, MODIS and VIIRS ocean color products (Chl-a and normalized fluorescence line height (nFLH)), MODIS lake ice products, Landsat images, gauged meteorological data and in situ spectral measurements, were used in this study. The data sources and processing methods are detailed below.

### 3.1. Ocean color products

MODIS Aqua level-2 data (Reprocessing 2014) were downloaded from the NASA Goddard Space Flight Center (GSFC, <https://oceancolor.gsfc.nasa.gov/>). All available data between 2003 and 2017 covering the

Qinghai Lake region were obtained (see location in Fig. 1); note that only ocean color data in warm months (from May to October), during which Qinghai Lake is completely free of ice, were used. The resulting dataset consists of over 5291 images. With a spatial resolution of 1 km, these images were projected onto the same cylindrical equidistant (rectangular) projection. The two products used in this study include Chl-a concentrations (in  $\text{mg m}^{-3}$ ) and the nFLH (in  $\text{mW cm}^{-2} \mu\text{m}^{-1} \text{sr}^{-1}$ ) because they represent the most important indicators for primary production that can be obtained using satellite remote sensing. The current NASA default Chl-a products were derived using two algorithms ([https://oceancolor.gsfc.nasa.gov/atbd/chlor\\_a/](https://oceancolor.gsfc.nasa.gov/atbd/chlor_a/)): the color index (CI) algorithm for oligotrophic water ( $\text{Chl-a} < 0.15 \text{ mg m}^{-3}$ ) (Hu et al., 2012a) and the standard blue-to-green band ratio algorithm for waters with larger Chl-a values (O'Reilly et al., 1998). Nevertheless, because the Chl-a values in Qinghai Lake are typically much larger than  $0.15 \text{ mg m}^{-3}$ , the Chl-a concentration therein was expected to be estimated using the latter method (Bi et al., 2018). The mathematical form of the MODIS nFLH was designed to be a baseline height calculation, and it uses the normalized water-leaving radiance at three red bands (i.e., 667, 678 and 748 nm) (Behrenfeld et al., 2009).

The nFLH was used to complement the Chl-a concentration because the calculations of the latter tend to be confounded by the presence of colored dissolved organic matter (CDOM) and/or sediments in the water column. The absorption maxima of CDOM and inorganic/organic particles are located in the blue spectral domain (Babin et al., 2003; Gitelson et al., 2008), and the blue-to-green ratio decreases with increasing concentrations of particles and CDOM, leading to Chl-a overestimations. Therefore, because CDOM has limited absorption at red spectral bands, the nFLH is immune to disturbances by CDOM (Babin et al., 2003; Gitelson et al., 2008). To further minimize the residual impacts of suspended sediments on the nFLH, the algal bloom index (ABI, in  $\text{mW cm}^{-2} \mu\text{m}^{-1}$ ) proposed by Hu and Feng (2017) was used in this study, and it can be estimated as follows:

$$\text{ABI} = \text{nFLH} / (1 + [R_{\text{rs},547} - 0.0015] \times \alpha) \quad (1)$$

where the remote sensing reflectance at 547 nm ( $R_{\text{rs},547}$ ) of clear water is approximately a constant of 0.0015 (Hu et al., 2013), and the term  $[R_{\text{rs},547} - 0.0015]$  is essentially the elevated reflection at 547 nm due to increased water turbidity. After scaling by an empirical factor  $\alpha$  (determined to be 80), Eq. (1) has been proven to be an effective method for reducing the effects of sediments on the nFLH (Hu and Feng, 2017).

For each year, the annual mean Chl-a, nFLH and ABI were estimated as the mean value of all ice-free months (May through October) in each year instead of the entire year. Note that, despite the advantages of the ABI, analyses of the Chl-a concentration and nFLH were also included in this study because NASA distributes standard Chl-a and nFLH ocean color products; moreover, these parameters are commonly accepted by the scientific community to represent the primary production of surface water (Behrenfeld et al., 2009). Ocean color observations are prone to contamination by environmental interruptions and/or nonoptimal observational conditions (sunglint, stray light, large view angles, etc.); thus, the *l2\_flags* of each level-2 file were further employed to discard low-quality datasets when composing monthly level-3 products. Specifically, the NASA quality control system (<https://oceancolor.gsfc.nasa.gov/atbd/ocl2flags/>) was used to generate monthly Chl-a and nFLH (ABI) products, and only data not associated with any of the predefined quality control flags were used. Detailed information about the quality control system can be found in Hooker et al. (2003) and Feng and Hu (2015). Indeed, because the nFLH is more prone to environmental contamination than Chl-a, two additional flags were used for the former ("MODGLINT" represents moderate sun glint contamination, and "PRODWARN" represents diffuse attenuation ( $K_{d,490}$ ) out of a meaningful range).

Ocean color products from MODIS Terra and VIIRS were also downloaded and used to examine whether these independent

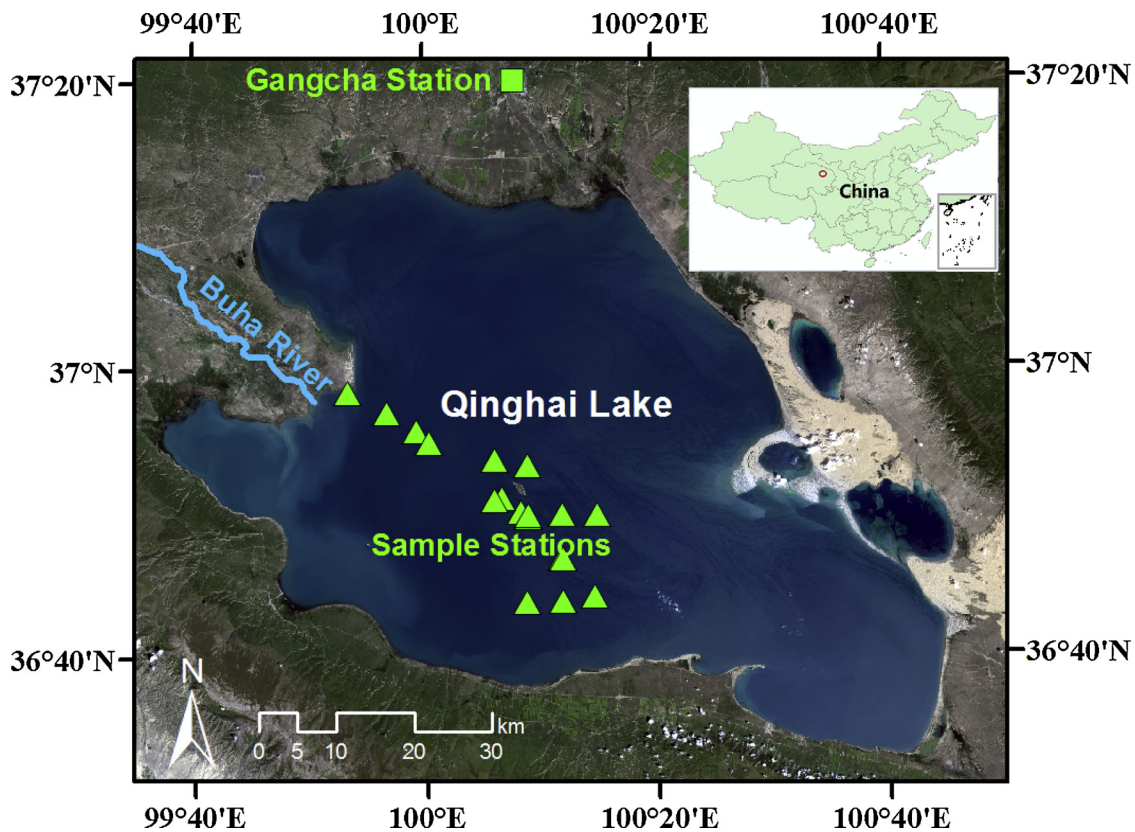


**Fig. 1.** Locations of Qinghai Lake (red circle in the inset), in situ sampling stations (triangle) and the nearest meteorological gauge station (green square). The location of the largest tributary (Buha River) is also indicated. The background is a red-green-blue true color composite image generated using Landsat 8 OLI data collected on August 10, 2015.

measurements were consistent with those of MODIS Aqua. MODIS Terra images encompassing the same period as that of MODIS Aqua (May through October 2003–2017, 5291 images) were obtained, whereas VIIRS images were not available until 2012 (~2000 images). The MODIS Terra and VIIRS data were projected onto the same cylindrical equidistant projection and the same spatial resolution (1 km) as MODIS Aqua. MODIS Terra datasets have both Chl-a and nFLH products; accordingly, the associated ABI products were also estimated using Eq. (1). In contrast, the nFLH and ABI products were not available for VIIRS due to the absence of a fluorescence band (Qi et al., 2015; Wang et al., 2013).

### 3.2. MODIS lake ice data

MODIS Terra daily snow cover products (MOD10A1) were downloaded from NASA (<https://modis-snow-ice.gsfc.nasa.gov/>) and used to monitor ice cover changes in Qinghai Lake over the period of study. With a spatial resolution of 500 m, the accuracy of MOD10A1 data is ~93% (Hall and Riggs, 2007). The freeze-up period (or ice-covered period) for each year was estimated as the ablation start date of the current year minus the freeze completion date of the previous year (the freeze completion date of some years even occurred in the current year). Following Kropáček et al. (2013), an ice cover threshold of 95% was used to determine when the lake was completely frozen, as speckle noises or algorithm errors tended to prevent 100% ice cover throughout certain years. Therefore, using the daily snow cover products, the ablation start date was determined as the time in the early period of the current year when the lake ice cover started to fall below 95%, and the freeze completion date was determined as the time in the later period of the previous year (or even very early in the current year) when the lake ice cover rose above 95%.

### 3.3. Meteorological data

Meteorological data collected at the nearest gauge station (Gangcha station, see Fig. 1) were downloaded from the China Meteorological Data Sharing Service System (<http://cdc.cma.gov.cn/>) over the same time span as the satellite observations. The meteorological measurements included the air temperature, number of sunshine hours, precipitation and wind speed, which are considered the most critical factors affecting the growth of phytoplankton (Hodges et al., 2000; Schindler and Nighswander, 1970; Agawin et al., 2000).

### 3.4. Landsat images

Cloud-free Landsat 5 Thematic Mapper (TM) and Landsat 8 Operational Land Imager (OLI) images between 2003 and 2017 were also downloaded from the United States Geological Survey (USGS) Land Processes Distributed Active Archive Center (LP DAAC) to extract the inundation area for Qinghai Lake. The data selection was confined to between May and September for each year to eliminate seasonal changes in the surface area. For each Landsat image, both normalized difference vegetation index (NDVI) images and red-green-blue true color images were generated to select the optimal NDVI thresholds to delineate the water/land boundaries of Qinghai Lake. Thresholds for a single spectral band (such as the near-infrared (NIR) band) or other band combinations, such as the normalized difference water index (NDWI) or modified NDWI (MNDWI), are also useful for water extraction, primarily due to the significant contrast between land and water (Zhang et al., 2017). The inundation areas were calculated by the number of pixels multiplied by the pixel size (i.e.,  $30 \times 30 \text{ m}^2$ ).

### 3.5. In situ spectral measurements

Cruise surveys were carried out on August 23<sup>rd</sup> and 24<sup>th</sup> 2014 to collect field data. Unfortunately, difficult field conditions impeded the proper storage and processing of water samples for Chl-a analysis; thus, only spectral data were successfully measured for the sampling stations (see Fig. 1). The instrument used for spectral measurements was the GER-2500 spectrometer (manufactured by the Spectra Vista Corporation from the USA), which has a spectral range of 350 nm to 1050 nm. The ocean optics protocol for above-water spectral measurements recommended by NASA was adopted during the in situ data collection (Mueller et al., 2003; Mobley, 1999). The upward radiance ( $L_u$ ), downward sky radiance ( $L_{sky}$ ), and radiance of a standard reference plaque ( $L_p$ ) were measured for each spectral measurement. Then, the  $R_{rs}$  value was estimated as follows:

$$R_{rs} = \rho_p(L_u - \rho_f \times L_{sky}) / \pi L_p \quad (2)$$

where the atmospheric reflection  $\rho_f$  was assumed to be 0.022 (Mobley, 1999), and  $\rho_p$  is the reflectance of the plaque provided by the manufacturer.

Concurrent MODIS Aqua  $R_{rs}$  retrievals and in situ reflectance data were also selected following the convention of Bailey and Werdell (2006) to gauge the performance of the atmospherically corrected  $R_{rs}$ . In this method, the satellite and in situ measurements are considered concurrent only if the time difference is within 3 h. Furthermore, to avoid spatial heterogeneity, the data selection was based on a coefficient of variation (i.e., standard deviation/mean) of less than 0.15 for the  $3 \times 3$  MODIS pixel window centered on the in situ point.

## 4. Results

Maps of the annual mean Chl-a between 2003 and 2017 are shown in Fig. 2, and the annual mean Chl-a concentrations estimated for the entire lake are plotted in Fig. 3. Note that the annual mean Chl-a represents the mean value during ice-free months (May through October) in each year instead of an entire year. Spatially, the Chl-a concentrations were greater in the near-shore regions than in the offshore areas, especially in the bay southwest of the Buha River Delta, where Chl-a

showed consistently higher values than most of the other parts of the lake. In terms of its temporal dynamics, Chl-a demonstrated significant interannual changes. The Chl-a values were relatively small in 2003 and 2004, in which bluish colors dominate most of the lake with a mean Chl-a value of  $\sim 1.5 \text{ mg m}^{-3}$ . In the subsequent years of 2005 and 2006, a prominent increase was observed (greenish to yellowish colors), and the MODIS Chl-a decreased to its previous levels between 2007 and 2013 with a slight increase in 2012. A remarkable increase in Chl-a was detected in 2014, and the highest value occurred in 2015 ( $4.3 \text{ mg m}^{-3}$ ), representing an approximately threefold increase over the previous years with normal Chl-a values.

Discernable disparities were found between the changing patterns of the Chl-a concentration and nFLH (see Fig. 4). The nFLH values remained relatively stable between 2003 and 2012 (with an annual mean value for the entire lake of  $\sim 0.09 \text{ mW cm}^{-2} \mu\text{m}^{-1} \text{ sr}^{-1}$ ), whereas Chl-a noticeably increased in 2005 and 2006. Therefore, the elevation of the satellite-derived Chl-a values in 2005 and 2006 may be associated with an increase in CDOM or sediment concentrations rather than with a real change in primary production. This is because the presence of CDOM can lead to overestimations of Chl-a when the OC3 Chl-a algorithm is used (Babin et al., 2003; Szeto et al., 2011). Although Chl-a has been increasing since 2014, a significant increase in the nFLH started one year earlier, and the mean nFLH of the second period (2013–2017) exceeded the 2003–2012 mean by  $\sim 45\%$ . Moreover, although smaller in magnitude, the interannual variability of ABI was found to mimic that of the nFLH (Figs. 3 and 5). The increase after 2013 was also pronounced, and the mean ABI from 2013 to 2017 was substantially higher (61%) than that in previous years. Indeed, although these ocean color products showed different fluctuations over the observed period of 2003–2017, a rapid increase in primary production was evident during recent years in Qinghai Lake, as is demonstrated by increases in Chl-a, nFLH and ABI. Notably, the maps of the annual mean nFLH and ABI (Figs. 4 and 5) seem to be noisier than those of the annual mean Chl-a due to the signal-to-noise ratios of the red bands being lower than those at shorter wavelengths (Hu et al., 2012b).

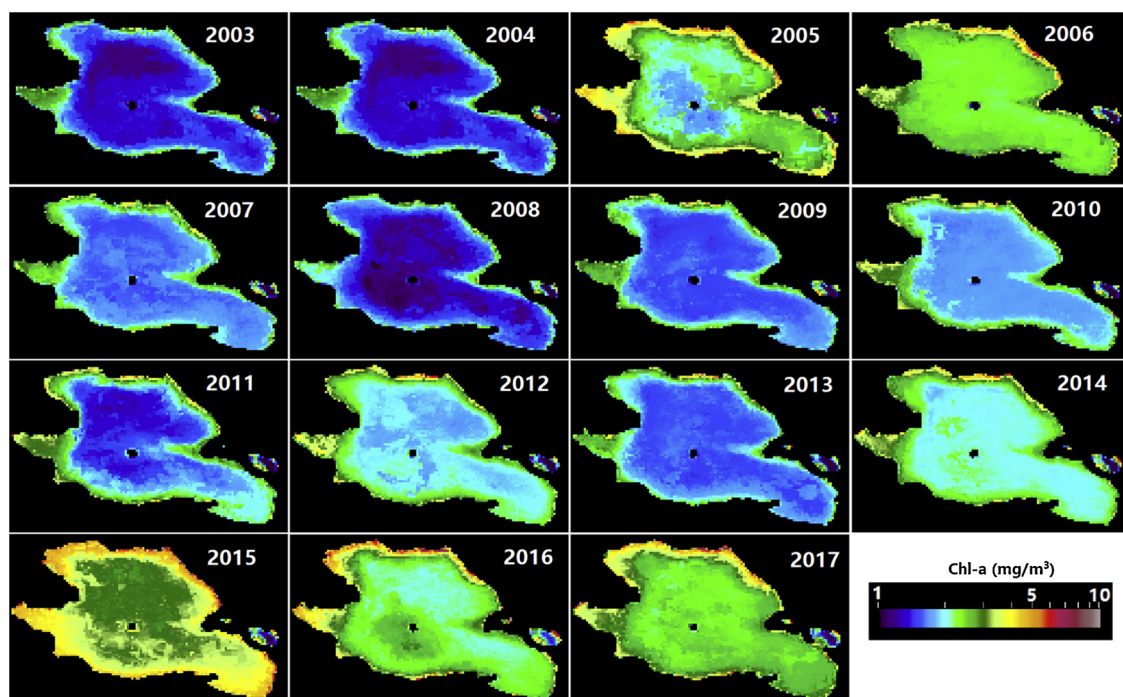


Fig. 2. Maps of the annual mean Chl-a concentration from 2003 to 2017. A significant increase can be found subsequent to 2013.

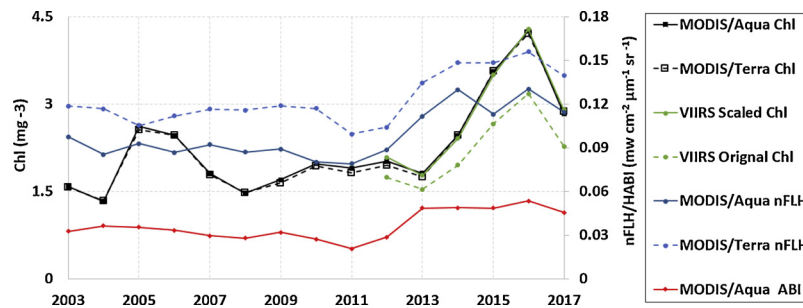


Fig. 3. Interannual changes in the Chl-a concentration, nFLH and ABI from three independent satellite ocean color missions (MODIS Aqua, MODIS Terra and VIIRS).

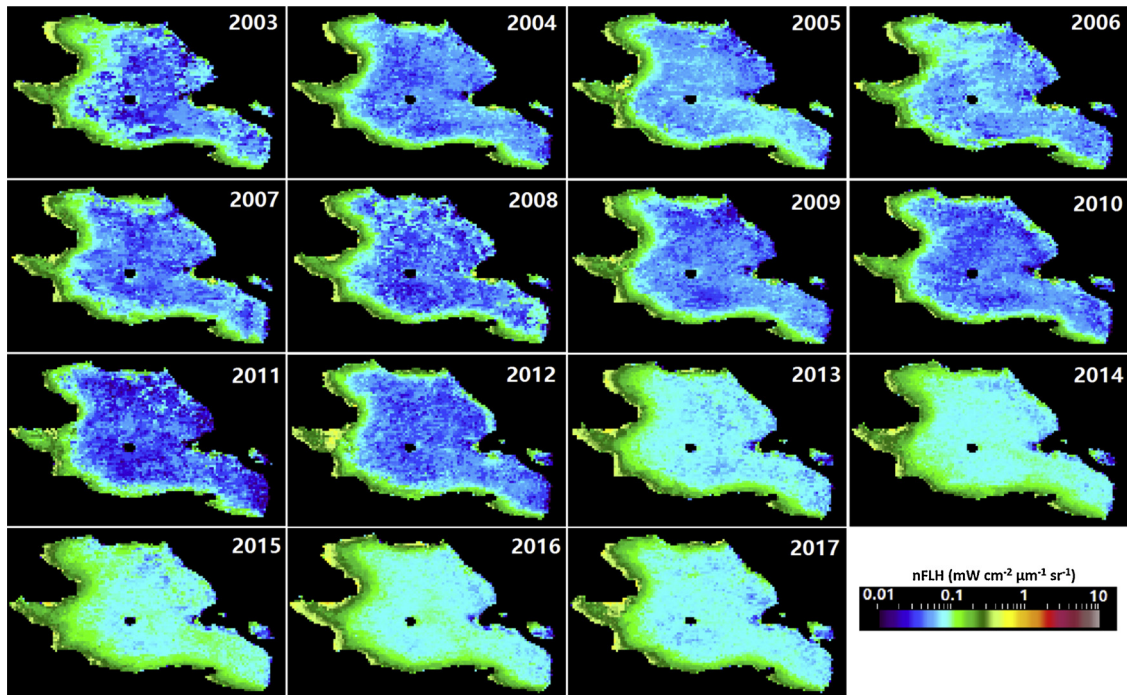


Fig. 4. Maps of the annual mean nFLH from 2003 to 2017. A significant increase can be found subsequent to 2012.

## 5. Discussion

### 5.1. Validity of the results

The long-term satellite observations presented herein demonstrated a rapid increase in primary production in Qinghai Lake in recent years. However, two types of uncertainties may have also contributed to the Chl-a and nFLH estimations: degradation of the instruments (Franz et al., 2007) and residuals errors in the atmospheric corrections (Hu et al., 2013). To eliminate potential misinterpretations of the interannual changes caused by these uncertainties, the following procedures were conducted.

First, ocean color products from two additional independent instruments (MODIS Terra and VIIRS) were similarly analyzed and compared; the processing methods were the same as those used for MODIS Aqua. The two MODIS instruments showed very similar results for all ocean color products. Specifically, the annual mean Chl-a values were generally identical between the two independent observations. Although the MODIS Terra nFLH values were consistently higher than the MODIS Aqua nFLH values, the interannual dynamics between the two sensors were analogous. In contrast, the VIIRS Chl-a estimates appeared to be systematically smaller than the MODIS Aqua Chl-a estimates; this was probably due to differences in their band configurations and spectral responses. However, strong correlations were found between the VIIRS and MODIS-derived Chl-a in terms of the monthly

mean values of the entire lake and their spatial patterns (Fig. 6a & b). A linear correction was used to scale the VIIRS Chl-a values to the same levels of the MODIS Aqua Chl-a values (solid green line in Fig. 3) based on the linear relationship between the monthly Chl-a values observed by the two instruments (Fig. 6a). Therefore, the impact of the degradation of the MODIS Aqua sensor on the long-term patterns of primary production in Qinghai Lake should be limited because it is unlikely that all three independent satellite missions degraded comparably during the study period.

Second, satellite  $R_{rs}$  retrievals derived using the standard atmospheric correction method (Gordon and Wang, 1994) were validated using sporadic in situ measurements. As demonstrated in Fig. 8, the MODIS  $R_{rs}$  values were consistent with the field-measured spectra in terms of both their magnitude (Fig. 8a) and their spectral shape (Fig. 8b). The uncertainties, represented using either the root mean square error or the mean relative error, were ~10%, and the mean ratio between them was 1.02. Indeed, such uncertainty levels for individual images would be significantly reduced if monthly or annual mean datasets were aggregated. In fact, the removal of the reflectance of aerosols over the Tibetan Plateau could be as accurate as that over the open ocean (Hu et al., 2013) due to the considerable distance of the plateau from human activities. Thus, atmospheric correction errors can be considered negligible when interpreting the significant increase in the Chl-a concentration (~three-fold) and nFLH (~45%).

To examine whether the threshold (i.e., 95%) used to determine a

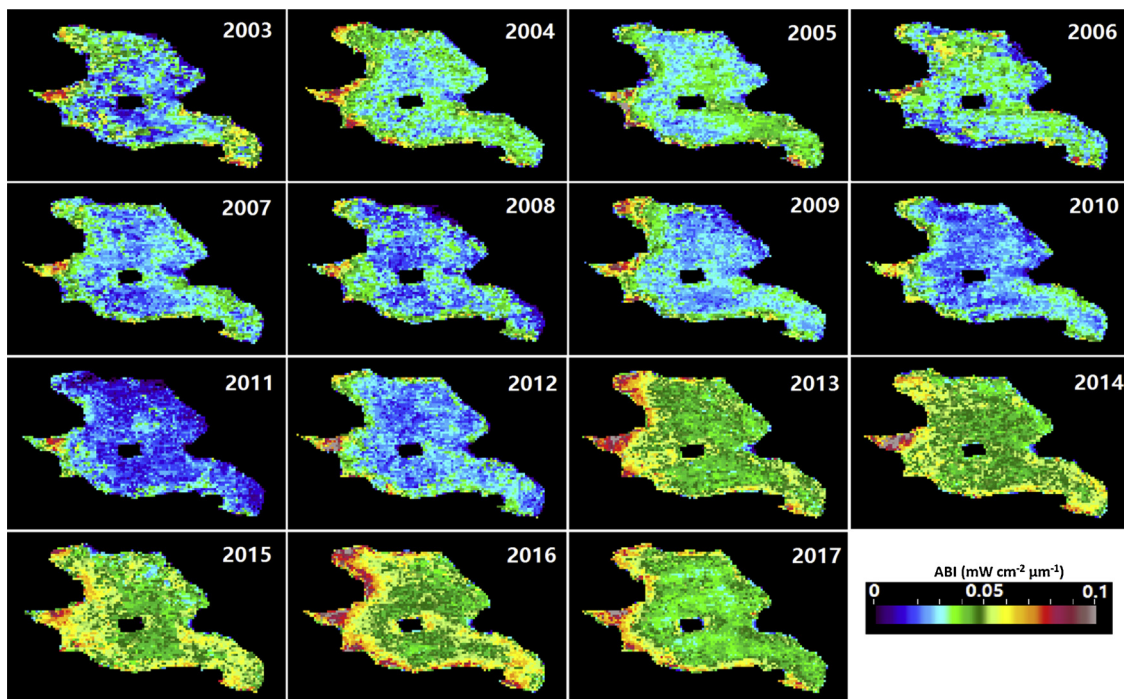


Fig. 5. Maps of the annual mean ABI from 2003 to 2017. A significant increase can be found subsequent to 2012.

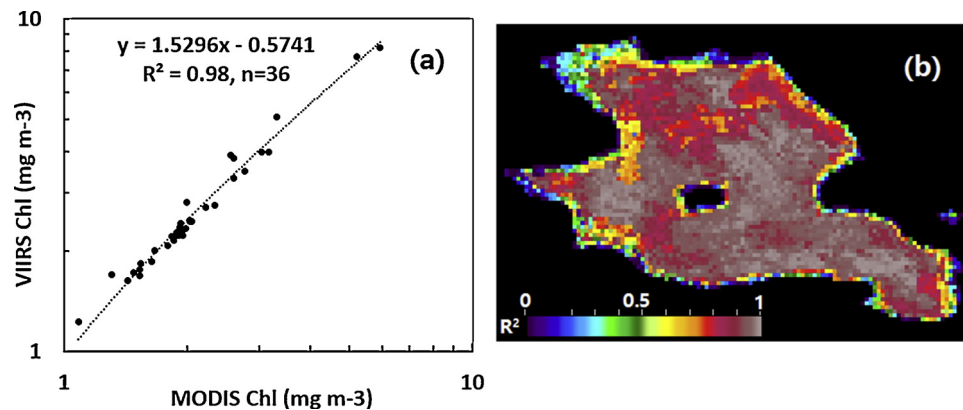


Fig. 6. Relationships between MODIS and VIIRS between 2013 and 2017. (a) Correlations between the monthly mean Chl-a of the entire lake. (b) Spatial correlations between the monthly mean Chl-a, where the pixel values represent the  $R^2$  between the monthly Chl-a concentrations of VIIRS and MODIS between 2013 and 2017.

“completely frozen” state could impact the freeze-up period, a sensitivity analysis was conducted using a threshold of 90% instead of 95%. When 90% was used as the threshold to classify the freeze-up period, the resulting changing patterns were very similar to those shown in Fig. 7a, and a high correlation was found ( $R^2 = 0.88$ ) between the two series of annual freeze-up periods derived using these different thresholds. Validations by Kropáček et al. (2013) showed that the (ice-free) open water date of Nam Co (a large lake atop the Tibetan Plateau) derived using 500 m MODIS snow products agreed very well (with a mean difference of 1.2 days) with that derived using time series of high-resolution optical and synthetic aperture radar (SAR) images. Therefore, the freeze-up period obtained with the MODIS snow products should be considered valid in this study. It is acknowledged that the freeze-up period would ideally be validated using ground truth data; however, considering the large size of the lake and the severe winter weather that strikes the local area, it is extremely difficult to conduct field surveys. Nevertheless, with increases in the availability of higher-resolution satellite datasets (such as the Sentinel series from the European Space Agency (ESA) and the Gaofen satellite series from China) (Feng et al., 2016), the ice cover and thus the freeze-up period on such

lakes can be estimated more accurately in the future.

### 5.2. Association with lake ice cover changes

The correlations between the annual mean ABI and the freeze-up period as well as four meteorological parameters (air temperature, number of sunshine hours, precipitation and wind speed) were analyzed (see the correlation coefficients in Table 1). As mentioned previously, the ABI was used instead of the Chl-a concentration or nFLH because the ABI is tolerant of the impacts of CDOM and suspended sediments. The temperature and availability of light constitute obvious constraints on primary production; precipitation and wind speed data are also analyzed because of their roles in regulating nutrients, as the former affects the surface runoff and nutrient discharge from terrestrial areas (Schindler and Nighswander, 1970) and the latter influences stratification and vertical nutrient mixing in the water column (Hodges et al., 2000). The relationships between each pair of the examined factors were estimated and tabulated accordingly.

The results showed that the ABI was negatively correlated with the freeze-up period during the observed timeframe, and their relationship

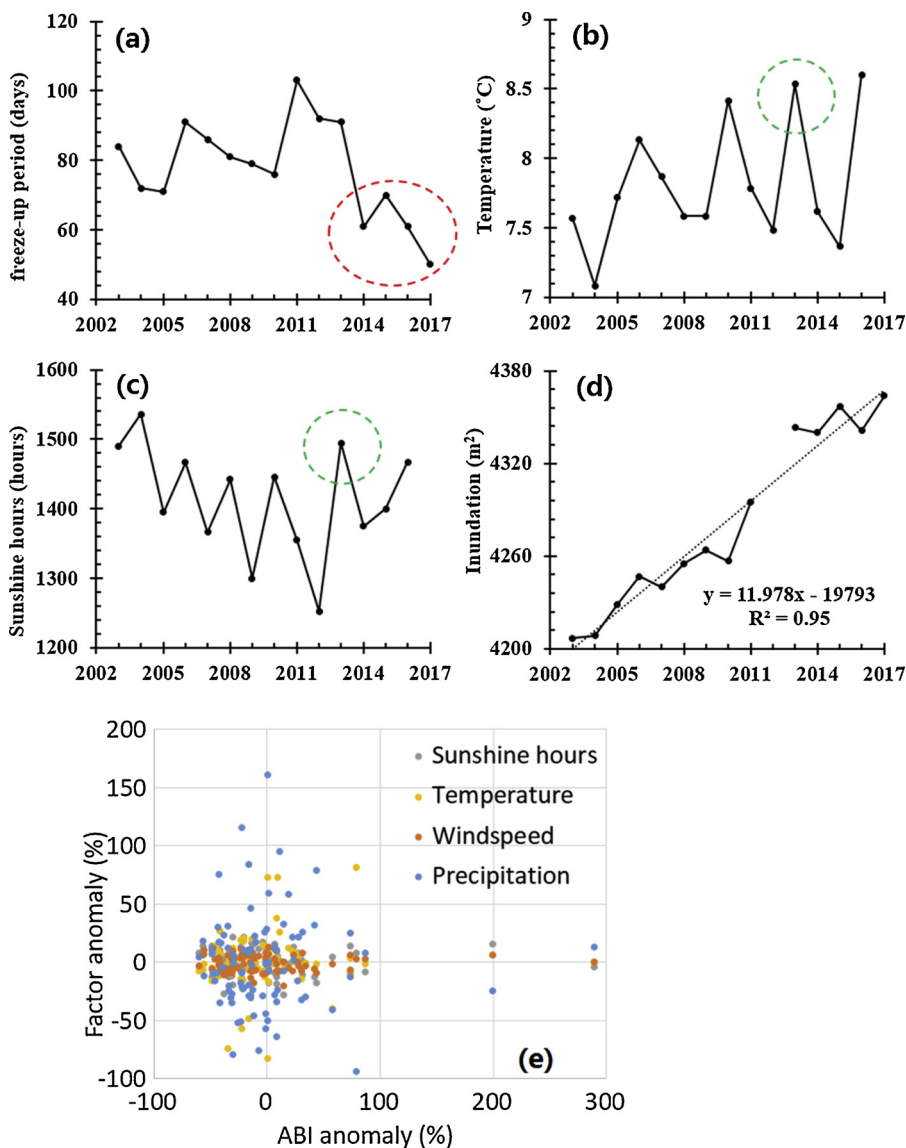


Fig. 7. Interannual changes in the freeze-up period (a), temperature (b), number of sunshine hours (c) and inundation area (d, valid high-quality Landsat data were not available in 2012 due to the scan line corrector failure of the Enhanced Thematic Mapper Plus (ETM+) instrument) from 2003 to 2017. (e) Scatter plots between monthly ABI anomalies (estimated as the relative departure from the monthly mean values) and the corresponding anomalies of four driving factors. The prominent decrease of freeze-up period after 2013 is red-circled in (a), and the high values in temperature and the number of sunshine hours in 2013 are green-circled in (b) and (c).

was statistically significant ( $R = -0.67$ ,  $p < 0.05$ ). This phenomenon appeared to be very similar to that observed in the Arctic Ocean, where marine primary production was boosted due to a reduction in ice cover (Arrigo et al., 2008; Horvat et al., 2017). The underlying mechanism is the melting of ice, which could increase light availability and thus promote photosynthesis and the growth of pelagic phytoplankton (Horvat et al., 2017). A plot of the freeze-up period (Fig. 7a) shows fluctuations between 2002 and 2013 with a mean value of  $84.2 \pm 9.7$  days. A prominent decrease can be observed after 2013; the 2014–2017 mean ( $60.5 \pm 8.2$  days) was statistically significant (i.e.,  $> 2$  times standard deviations below “normal”) and lower than that of the first period. The general trends in these results (i.e., an earlier ablation date and a delayed freeze-up date) are similar to those of Cai et al. (2017). The differences in the absolute values can be attributed to differences in the resolutions of the satellite data sources (500 m resolution for MODIS versus 25 km resolution for microwave imagery).

Nevertheless, although the dynamics of the freeze-up period mimic those of the ABI, one puzzle still remains: the decrease in the ice cover duration that occurred one year after the significant increase in the ABI. Indeed, when examining the long-term trends in the other climatic factors, both the temperature and the number of sunshine hours were high in 2013 (Fig. 7b & c); therefore, the high ABI in this year was likely associated with favorable weather conditions. However, since the

changes in the ABI were uncorrelated with the long-term variations in either of these individual factors, their effect of enhancing the ABI could occur only when both values are high.

Other factors, including the accelerated melting of glaciers and permafrost in the Tibetan Plateau region due to the effects of global warming (Kuang and Jiao, 2016), could have influenced the primary productivity in Qinghai Lake and could have led to a rapid expansion in the inundation area in recent years (Song et al., 2014; Zhang et al., 2011). More minerals and chemicals (e.g., phosphorus, silicate and iron) are assumed to be discharged into the lake as a result of this melting (Hawkings et al., 2015), favoring the growth of phytoplankton. However, the increasing trend in the surface area of Qinghai Lake can be observed throughout the entire period of study (Fig. 7d), which makes the abrupt increase in the ABI after 2013 difficult to explain. Likewise, although anthropogenic factors (such as human settlement and agriculture along the lake) may have also influenced the nutrient input and thus may have also changed the productivity of the water column in Qinghai Lake, the gradual changes of these effects make it difficult to explain the sudden increase in the ABI.

The relative contributions of the three primary factors (i.e., the freeze-up period, number of sunshine hours, and temperature) to the interannual changes in the ABI were estimated using a multiple general linear model (GLM). In the GLM, annual data of the freeze-up period,

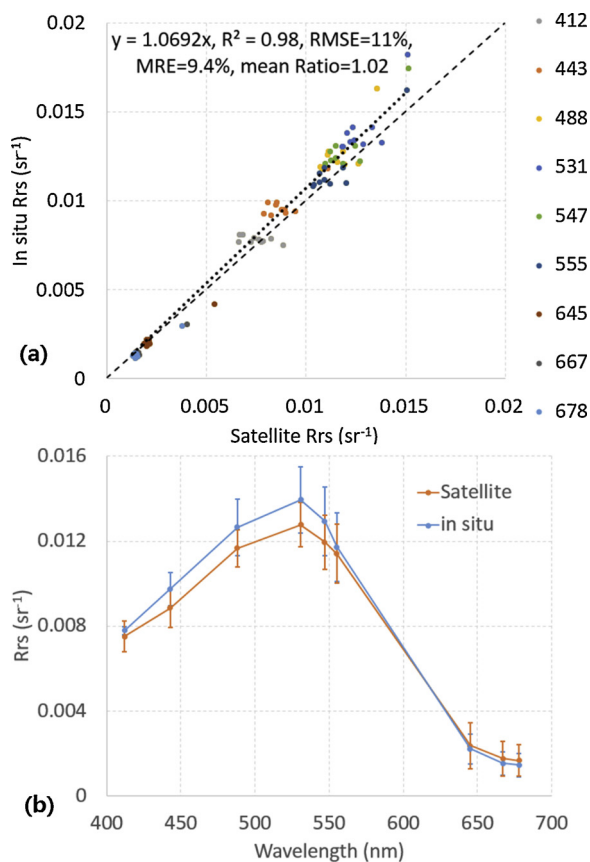


Fig. 8. Comparison of the (a) magnitudes and (b) spectral shapes (the vertical bars represent standard deviations) between the atmospherically corrected MODIS  $R_{rs}$  and in situ measurements.

number of sunshine hours, and temperature were used as independent variables, and the corresponding annual mean ABI values were used as the dependent variable; the outputs of the model were the relative contributions of the independent variables. The results indicated that the freeze-up period, number of sunshine hours, and temperature explained 76.1%, 5.6%, and 10.2%, respectively, of the long-term changes in the ABI throughout Qinghai Lake between 2003 and 2017, and the remaining 8.1% was correlated with other unknown factors. Moreover, when ordinary least squares (OLS) regression was used to predict the ABI using the freeze-up period, number of sunshine hours, and temperature, the resulting correlation was also statistically significant ( $R^2 = 0.53$ ,  $p = 0.04$ ). The OLS regression p-values are listed in Table 1 for each of the three factors; only the freeze-up period was within the 95% confidence level ( $p = 0.02$ ), further indicating its critical role in modulating the growth of phytoplankton in Qinghai Lake. The exclusion of the wind speed and precipitation from both the GLM and the

Table 1

Correlation coefficient matrix between the ABI and five driving forces. The last line demonstrates the relative contributions (estimated using a GLM) of the three primary factors to the interannual changes in the ABI, and the last column shows the residual contributions from other factors. The last row shows the p-value for each factor when OLS regression was used to predict the ABI using these factors.

	ABI	Freeze-up period	Sunshine hours	Temperature	Windspeed	Precipitation	Residuals
ABI		-0.67*	0.32	0.54	0.12	0.57*	-
Freeze-up period			-0.22	0.05	-0.25	-0.63*	-
Sunshine hours				0.25	0.57*	0.01	-
Temperature					-0.19	0.24	-
Wind speed						0.04	-
Precipitation							-
Relative contribution (%) (GLM)		76.1	5.6	10.2	-	-	8.1
p-value (OLS)		0.02	0.63	0.29	-	-	-

OLS analysis is because they were significantly correlated with one or more of the three primary factors (see Table 1). However, further efforts are required to understand the significant correlations between the different climatic variables.

To examine the impacts of the four meteorological factors (the number of sunshine hours, temperature, precipitation and wind speed) on the ABI at the monthly scale, the correlations between the deseasonalized long-term ABI and these parameters were also examined. The deseasonalized data were represented as monthly anomalies, and the data for each month were estimated as the relative difference between the mean of the current month and the climatological mean value for that month (i.e., the monthly mean values between 2003 and 2017). The results indicated that the changing patterns of the ABI anomalies differed from those of the examined factors, and there was no significant correlation between the monthly ABI anomalies and either of the driving factors. Therefore, the dynamics of phytoplankton growth in Qinghai Lake at the monthly scale could not be related to these climatic variables, while their impacts were evident at the annual scale. This phenomenon could possibly be due to the time lag of the impacts of climate change on phytoplankton growth in Qinghai Lake, while such impacts could be accumulated at the annual scale (Knowles, 2002).

Another interesting finding was that the freeze-up period was uncorrelated with the air temperatures between 2003 and 2017 (see Table 1). However, this kind of correlation does not mean that temperature has no impact on lake ice formation. A possible cause of this phenomenon is that the complete freeze-up of the lake is a combined effect of temperature, precipitation (significantly correlated with the freeze-up period, see Table 1) and many other meteorological conditions, and this process could be abrupt rather than gradual. The exact mechanism requires further investigation once additional meteorological and biogeochemical data become available. Nevertheless, with a continuous increase in temperature and accelerated ice melting (Zhou and Yu, 2006), the dynamics of primary production in Qinghai Lake and other Tibetan Plateau lakes are expected to become more significant in the future (Cai et al., 2017).

### 5.3. Future implications

The method and findings presented in this study have significant implications for studying the biogeochemical characteristics of similar water bodies worldwide, particularly with the help of multiple satellite mission products. With the current global warming background, the surface areas of global alpine lakes have experienced significant changes (either expansion or shrinkage) (Pekel et al., 2016; Smith et al., 2005; Song et al., 2014). Superimposed on these rapid hydrological dynamics could be considerable alterations in the biogeochemical properties of lake water. Due to the free availability of various remote sensing products (e.g., the ocean color and ice cover products in this study), the approach used herein could be easily extended to other alpine lakes or estuarine regions to study the climate- or human-induced changes in water primary production and other parameters.

## 6. Conclusion

Ocean color products from MODIS Aqua, MODIS Terra and VIIRS have been used to study the changes in the primary production in Qinghai Lake, which is situated at a high altitude atop the Tibetan Plateau. Observations from three satellite missions showed consistent increases in the Chl-a concentration, nFLH and ABI in recent years, clearly indicating a phytoplankton bloom. The freeze-up period was significantly correlated with primary production, and other environmental factors (the temperature and the number of sunshine hours) could also modulate the interannual changes. Nevertheless, understanding the decrease in ice cover still requires future investigation. To the best of the authors' knowledge, this is the first comprehensive assessment of the biogeochemical properties of Qinghai Lake. Furthermore, the methods used herein are extendable to other lakes throughout the Tibetan Plateau to study the potential impacts of climate change on the biological dynamics of alpine lakes.

## Acknowledgements

This work was supported by the Strategic Priority Research Program of Chinese Academy of Sciences, under grant XDA20060402, the National Natural Science Foundation of China under grants 41671338, 91747204, 41625001 and 41471308, the Youth Innovation Promotion Association of Chinese Academy of Sciences (2015128), the Guangdong Provincial Key Laboratory of Soil and Groundwater Pollution Control (No. 2017B030301012), the State Environmental Protection Key Laboratory of Integrated Surface Water-Groundwater Pollution Control, and the Southern University of Science and Technology under grant G01296001. We also acknowledge the extensive comments and suggestions from two anonymous reviewers.

## References

- Pekel, J.-F., Cottam, A., Gorelick, N., Belward, A.S., 2016. High-resolution mapping of global surface water and its long-term changes. *Nature* 540 (7633), 418.
- Kraemer, B., Mehner, T., Adrian, R., 2017. Reconciling the Opposing Effects of Warming on Phytoplankton Biomass in 188 Large Lakes.
- Smith, L.C., Sheng, Y., MacDonald, G.M., Hinzman, L.D., 2005. Disappearing arctic lakes. *Science* 308 (5727), 1429.
- Song, C., Huang, B., Richards, K., Ke, L., Hien Phan, V., 2014. Accelerated lake expansion on the Tibetan Plateau in the 2000s: induced by glacial melting or other processes? *Water Resour. Res.* 50 (4), 3170–3186.
- Liu, X., Chen, B., 2000. Climatic warming in the Tibetan Plateau during recent decades. *Int. J. Climatol.* 20 (14), 1729–1742.
- Shi, Y., Ren, J., 1990. Glacier recession and lake shrinkage indicating a climatic warming and drying trend in central Asia. *Ann. Glaciol.* 14, 261–265.
- Dong, H., Song, Y., 2011. Shrinkage History of Lake Qinghai and Causes During the Last 52 Years. pp. 446–449.
- Zhang, G., Xie, H., Kang, S., Yi, D., Ackley, S.F., 2011. Monitoring lake level changes on the Tibetan Plateau using ICESat altimetry data (2003–2009). *Remote Sens. Environ.* 115 (7), 1733–1742.
- Li, X.-Y., Xu, H.-Y., Sun, Y.-L., Zhang, D.-S., Yang, Z.-P., 2007. Lake-level change and water balance analysis at Lake Qinghai, West China during recent decades. *Water Resour. Manage.* 21 (9), 1505–1516.
- Cai, Y., Ke, C.-Q., Duan, Z., 2017. Monitoring ice variations in Qinghai Lake from 1979 to 2016 using passive microwave remote sensing data. *Sci. Total Environ.* 607, 120–131.
- Zhang, G., Xie, H., Yao, T., Li, H., Duan, S., 2014. Quantitative water resources assessment of Qinghai Lake basin using Snowmelt Runoff Model (SRM). *J. Hydrol.* 519, 976–987.
- Wenbin, Z., Jia, S., Lv, A., 2014. Monitoring the Fluctuation of Lake Qinghai Using Multi-Source Remote Sensing Data.
- Dong, H., Zhang, G., Jiang, H., Yu, B., Chapman, L.R., Lucas, C.R., Fields, M.W., 2006. Microbial diversity in sediments of Saline Qinghai Lake, China: linking geochemical controls to microbial ecology. *Microb. Ecol.* 51 (1), 65–82.
- Bi, R., Zhang, H., Li, H., Chang, F., Duan, L., He, Y., Zhang, H., Wen, X., Zhou, Y., 2018. Characteristics and changes of water quality parameters of Qinghai lake in 2015. *J. Water Resour. Res.* 7 (1), 74–83.
- McClain, C.R., 2009. A decade of satellite ocean color observations. *Ann. Rev. Mar. Sci.* 1, 19–42.
- Wang, M., Nim, C.J., Son, S., Shi, W., 2012. Characterization of turbidity in Florida's lake Okeechobee and Caloosahatchee and St. Lucie estuaries using MODIS-Aqua measurements. *Water Res.* 46 (16), 5410–5422.
- O'Reilly, J.E., Maritorena, S., Mitchell, B.G., Siegel, D.A., Carder, K.L., Garver, S.A., Kahru, M., McClain, C., 1998. Ocean color chlorophyll algorithms for SeaWiFS. *J. Geophys. Res. Oceans* 103 (C11), 24937–24953.
- Werdell, P.J., Bailey, S.W., 2005. An improved in-situ bio-optical data set for ocean color algorithm development and satellite data product validation. *Remote Sens. Environ.* 98 (1), 122–140.
- Immerzeel, W.W., Van Beek, L.P., Bierkens, M.F., 2010. Climate change will affect the Asian water towers. *Science* 328 (5984), 1382–1385.
- Rhode, D., Haizhou, M., Madsen, D.B., Brantingham, P.J., Forman, S.L., Olsen, J.W., 2010. Paleoenvironmental and archaeological investigations at Qinghai Lake, western China: geomorphic and chronometric evidence of lake level history. *Quat. Int.* 218 (1), 29–44.
- Colman, S.M., Yu, S.-Y., An, Z., Shen, J., Henderson, A.C.G., 2007. Late Cenozoic climate changes in China's western interior: a review of research on Lake Qinghai and comparison with other records. *Quat. Sci. Rev.* 26 (17), 2281–2300.
- Yan, J.P., Hinderer, M., Einsele, G., 2002. Geochemical evolution of closed-basin lakes: general model and application to Lakes Qinghai and Turkana. *Sediment. Geol.* 148 (1), 105–122.
- Hu, C., Lee, Z., Franz, B., 2012a. Chlorophyll algorithms for oligotrophic oceans: a novel approach based on three-band reflectance difference. *J. Geophys. Res. Oceans* 117 (C1).
- Behrenfeld, M.J., Westberry, T.K., Boss, E.S., O'Malley, R.T., Siegel, D.A., Wiggert, J.D., Franz, B., McLain, C., Feldman, G., Doney, S.C., 2009. Satellite-detected fluorescence reveals global physiology of ocean phytoplankton. *Biogeosciences* 6 (5), 779.
- Babin, M., Stramski, D., Ferrari, G.M., Claustre, H., Bricaud, A., Obolensky, G., Hoepffner, N., 2003. Variations in the light absorption coefficients of phytoplankton, nonalgal particles, and dissolved organic matter in coastal waters around Europe. *J. Geophys. Res. Oceans* 108 (C7).
- Gitelson, A.A., Dall'Olmo, G., Moses, W., Rundquist, D.C., Barrow, T., Fisher, T.R., Gurlin, D., Holz, J., 2008. A simple semi-analytical model for remote estimation of chlorophyll-a in turbid waters: validation. *Remote Sens. Environ.* 112 (9), 3582–3593.
- Hu, C., Feng, L., 2017. Modified MODIS fluorescence line height data product to improve image interpretation for red tide monitoring in the eastern Gulf of Mexico. *J. Appl. Remote Sens.* 11 (1), 012003.
- Hu, C., Feng, L., Lee, Z., 2013. Uncertainties of SeaWiFS and MODIS remote sensing reflectance: implications from clear water measurements. *Remote Sens. Environ.* 133, 168–182.
- Hooker, S., Firestone, E.R., Patt, F.S., Barnes, R.A., Eplee Jr, R.E., Franz, B.A., Robinson, W.D., Feldman, G.C., Bailey, S.W., 2003. Algorithm Updates for the Fourth SeaWiFS Data Reprocessing.
- Feng, L., Hu, C., 2015. Comparison of valid ocean observations between MODIS terra and aqua over the global oceans. *Geosci. Remote Sens. IEEE Trans.* 99, 1–11.
- Qi, L., Hu, C., Cannizzaro, J., Corcoran, A.A., English, D., Le, C., 2015. VIIRS observations of a *Karenia brevis* bloom in the Northeastern Gulf of Mexico in the absence of a fluorescence band. *IEEE Geosci. Remote. Sens. Lett.* 12 (11), 2213–2217.
- Wang, M., Liu, X., Tan, L., Jiang, L., Son, S., Shi, W., Rausch, K., Voss, K., 2013. Impacts of VIIRS SDR performance on ocean color products. *J. Geophys. Res. Atmos.* 118 (18), 10,347–10,360.
- Hall, D.K., Riggs, G.A., 2007. Accuracy assessment of the MODIS snow products. *Hydrol. Processes: Int. J.* 21 (12), 1534–1547.
- Kropáček, J., Maussion, F., Chen, F., Hoerz, S., Hochschild, V., 2013. Analysis of ice phenology of lakes on the Tibetan Plateau from MODIS data. *Cryosphere* 7, 287–301.
- Hodges, B.R., Imberger, J., Saggio, A., Winters, K.B., 2000. Modeling basin-scale internal waves in a stratified lake. *Limnol. Oceanogr.* 45 (7), 1603–1620.
- Schindler, D., Nighswander, J., 1970. Nutrient supply and primary production in Clear Lake, eastern Ontario. *J. Fish. Board Canada* 27 (11), 2009–2036.
- Agawin, N.S., Duarte, C.M., Agustí, S., 2000. Nutrient and temperature control of the contribution of picoplankton to phytoplankton biomass and production. *Limnol. Oceanogr.* 45 (3), 591–600.
- Zhang, G., Zheng, G., Gao, Y., Xiang, Y., Lei, Y., Li, J., 2017. Automated Water Classification in the Tibetan Plateau Using Chinese GF-1 WFV Data.
- Mueller, J.L., McClain, G.S.F.C.R., Mueller, J., Bidigare, R., Trees, C., Balch, W., Dore, J., Drapeau, D., Karl, D., Van, L., 2003. Ocean Optics Protocols For Satellite Ocean Color Sensor Validation, Revision 5, Volume V: Biogeochemical and Bio-Optical Measurements and Data Analysis Protocols. National Aeronautical and Space Administration Report 21621. pp. 1–72.
- Mobley, C.D., 1999. Estimation of the remote-sensing reflectance from above-surface measurements. *Appl. Opt.* 38 (36), 7442–7455.
- Bailey, S.W., Werdell, P.J., 2006. A multi-sensor approach for the on-orbit validation of ocean color satellite data products. *Remote Sens. Environ.* 102 (1–2), 12–23.
- Szeto, M., Werdell, P.J., Moore, T.S., Campbell, J.W., 2011. Are the world's oceans optically different? *J. Geophys. Res. Oceans* 116 (C7).
- Hu, C., Feng, L., Lee, Z., Davis, C.O., Mannino, A., McClain, C.R., Franz, B.A., 2012b. Dynamic range and sensitivity requirements of satellite ocean color sensors: learning from the past. *Appl. Opt.* 51 (25), 6045–6062.
- Franz, B.A., Bailey, S.W., Werdell, P.J., McClain, C.R., 2007. Sensor-independent approach to the vicarious calibration of satellite ocean color radiometry. *Appl. Opt.* 46 (22), 5068–5082.
- Gordon, H.R., Wang, M., 1994. Retrieval of water-leaving radiance and aerosol optical thickness over the oceans with SeaWiFS: a preliminary algorithm. *Appl. Opt.* 33 (3), 443–452.
- Feng, L., Li, J., Gong, W., Zhao, X., Chen, X., Pang, X., 2016. Radiometric cross-calibration of Gaofen-1 WFV cameras using Landsat-8 OLI images: a solution for large view angle associated problems. *Remote Sens. Environ.* 174, 56–68.
- Arrigo, K.R., van Dijken, G., Pabi, S., 2008. Impact of a shrinking Arctic ice cover on marine primary production. *Geophys. Res. Lett.* 35 (19).
- Horvat, C., Jones, D.R., Iams, S., Schroeder, D., Flocco, D., Feltham, D., 2017. The frequency and extent of sub-ice phytoplankton blooms in the Arctic Ocean. *Sci. Adv.* 3

- (3) e1601191.
- Kuang, X., Jiao, J.J., 2016. Review on climate change on the Tibetan Plateau during the last half century. *J. Geophys. Res. Atmos.* 121 (8), 3979–4007.
- Hawkings, J., Wadham, J., Tranter, M., Lawson, E., Sole, A., Cowton, T., Tedstone, A., Bartholomew, I., Nienow, P., Chandler, D., 2015. The effect of warming climate on nutrient and solute export from the Greenland Ice Sheet. *Geochem. Perspect. Lett.* 1, 94–104.
- Knowles, N., 2002. Natural and management influences on freshwater inflows and salinity in the San Francisco Estuary at monthly to interannual scales. *Water Resour. Res.* 38 (12) 25-21-25-11.
- Zhou, T., Yu, R., 2006. Twentieth-century surface air temperature over China and the globe simulated by coupled climate models. *J. Clim.* 19 (22), 5843–5858.